INTERNATIONAL JOURNAL FOR NUMERICAL METHODS IN FLUIDS, VOL. 4, 43–69 (1984)

AN 'ASSUMED DEVIATORIC STRESS–PRESSURE–VELOCITY' MIXED FINITE ELEMENT METHOD FOR UNSTEADY, CONVECTIVE, INCOMPRESSIBLE VISCOUS FLOW: PART II: COMPUTATIONAL STUDIES

CHIEN-TUNG YANG* AND SATYA N. ATLURI†

Center for the Advancement of Computational Mechanics, Georgia Institute of Technology, Atlanta, GA 30332, U.S.A.

SUMMARY

In Part I of this paper we presented a mixed finite element method, for solving unsteady, incompressible, convective flows, based on assumed 'deviatoric stress–velocity–pressure' fields in each element, which have the features: (i) the convective term is treated by the usual Galerkin technique; (ii) the unknowns in the global system of finite element equations are the nodal velocities, and the 'constant term' in the arbitrary pressure field over each element; and (iii) exact integrations are performed over each element.

In this paper we present numerical studies, both for steady as well as unsteady cases, of the problems: (a) the driven cavity, (b) Jeffry–Hamel flow in a channel, (c) flow over a 'backward' or 'downstream' facing step, and (d) flow over a square step. All these problems are two-dimensional in nature, although certain 3-D solutions are to be presented in a separate paper. The present results are compared with those which are available in the literature and are based on alternative approaches to treat incompressibility and convective acceleration. The possible merits of the present method are thus pointed out.

KEY WORDS Mixed Method Assumed Deviatoric Stress Galerkin Formulation

PROBLEM OF THE WALL-DRIVEN CAVITY

(a) *Steady-flow*

The problem definition is given in Figure 1. This problem has been analysed previously, using reduced-integration-penalty methods, by: (i) Hughes, Liu, and Brooks[1] using 4 noded bilinear velocity elements, with one-point integration for the penalty term, and 2×2 Gauss–Legendre rule for the convection terms (with no 'upwinding'). Their[1] finite element system involved 882 or 924 equations prior to the imposition of boundary conditions. Both the velocity and pressure solutions were presented.[1] (ii) Bercovier and Engelman[2] using 9-noded parabolic velocity elements, with 2×2 integration for the penalty term, and 3×3 integration for convection terms. The finite element system involved 964 equations before the imposition of the boundary conditions. Again, both velocity and pressure solutions are presented in Reference 1. (iii) Heinrich and Marshall[3] using 8 or 9 noded biquadratic

* Doctoral Candidate
† Regents' Professor of Mechanics

0271–2091/84/010043–27$02.70 *Received October 1982*

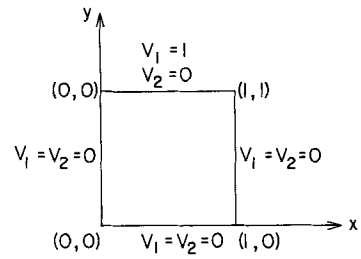

Figure 1. Problem definition for a 'driven cavity'

velocity elements, with 2×2 integration for the penalty term, and 3×3 integration for the convection term. The finite element system involved 1050 equations before imposition of the boundary conditions. Only velocity results are presented in Reference 3. The solutions in References 1–3 are two-dimensional in nature, as are the present. Some three-dimensional solutions are beginning to appear in the literature;[4,5] these will be compared with our results in a forthcoming paper.

It should be remarked however, that Oden *et al.*[6,7] find that the penalty-based 4 and 9 node elements using, respectively, 1 point and 2×2 point integration for the penalty term may lead to divergent pressure solutions which may need averaging or filtering to stabilize them.

In contrast, in the present method, 2 meshes as shown in Figure 2 are used. Mesh A consists of 88 four-noded elements and 108 nodes; and thus the finite element system involves $(2\times108+88)=304$ equations prior to the imposition of boundary conditions. Mesh B consists of 168 elements and 195 nodes, thus the number of equations is $(2\times195+168)=558$. From Figure 3, wherein the computed velocity profiles on the vertical centre line of the flow domain are shown for two different Reynolds numbers, i.e. $Re = 100$, and 400, it is seen that the results are insignificantly different for the two finite element meshes. In Figure 4, the present results are compared with those of Burgraff.[8] Even though the present results were insignificantly different for the meshes A and B of Figure 2, in order to generate 'resonably pretty looking' computer plots of velocity vectors and streamlines, Mesh B is

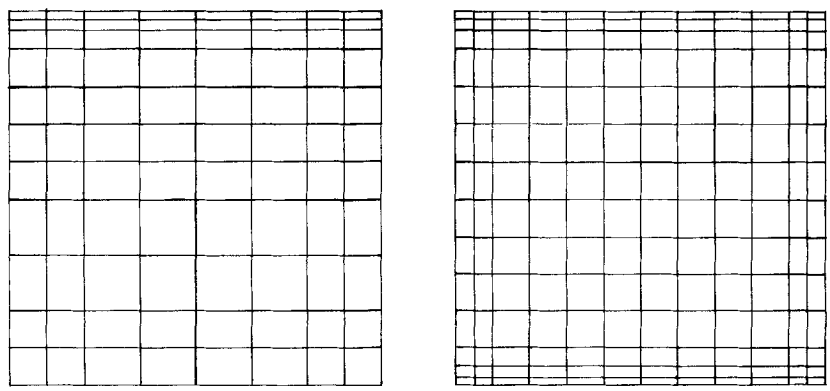

Figure 2. Finite element meshes for the driven cavity problem (A) Total number of elements = 88, Total number of points = 108; (B) Total number of elements = 168, Total number of points = 195

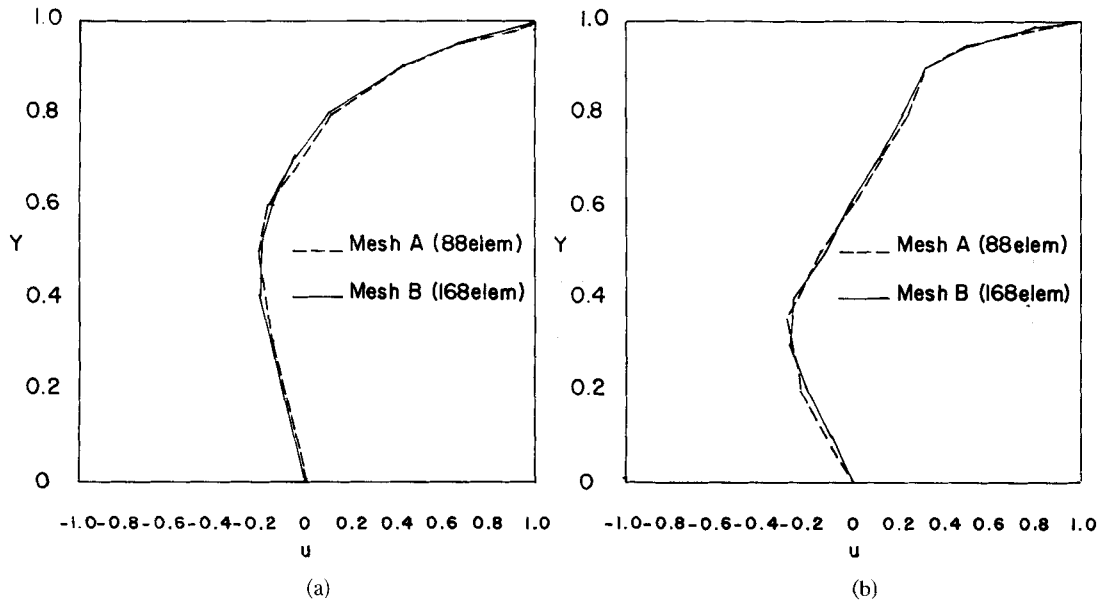

Figure 3. Velocity profiles on vertical centre line (comparison of 2 FE meshes): (a) $Re = 100$; (b) $Re = 400$

selected for the results to follow, since this will lead to 'dense' contours,* at least within the 'primitive' graphics capabilities that we have. Figures 5, 6 and 7 show, respectively, the velocity vector and stream line contours for $Re = 100$, 400 and 1000. Figure 8 shows the velocity vector plots for $Re = 2000$ and 3000, respectively. Figures 9, 10 and 11 show respectively, the computed pressure contours for $Re = 0$, 100; 400, 1000; and 3000. It should be remarked that the present method leads to a 'direct' computation of the pressure.

In order to study the effect of mesh distortion, Mesh B of Figure 2 has been distorted as shown in Figure 12(a), wherein 4 noded 'isoparametric' elements are used. The computed velocity vector profiles for $Re = 100$, 400 and 1000 are shown, for the distorted mesh, in Figures 12(b) and 13, respectively. Thus the present results are seen to be insensitive to mesh distortion.

Considering the excellent correlation of the present results for both velocity and pressure with those in References 1–3 and 8, and considering that the present method uses far fewer equations than in References 1–3, it is believed that the present results point to the relative efficiency of the present method.

(b) *Unsteady-flow*

A solution to the transient problem of the driven cavity has been recently presented by Donea *et al.*[9] who used a velocity–pressure formulation and a 'fractional step' approach to the time-integration in which only the incompressibility condition is treated implicitly. A non-uniform 20×20 mesh of 4-noded elements with bilinear velocity and constant pressure was employed.[9] Thus, the total number of finite element equations, prior to imposition of boundary conditions, appears to be 1282 in Reference 9. The transient problem was solved for $Re = 1000$ and results shown for $t = 5$, 10, 15 s in Reference 9.

* Here, and in what follows, plots of velocity vectors along element edges as well as in the interior are given.

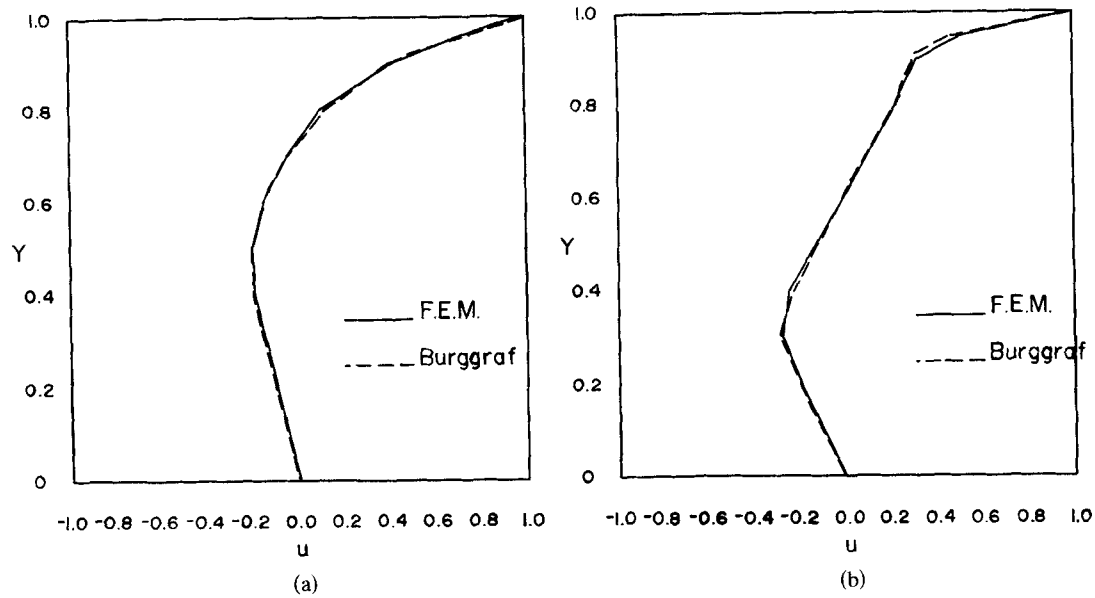

Figure 4. Velocity profiles on vertical centre line for driven cavity flow (comparison with finite difference results): (a) $Re = 100$; (b) $Re = 400$

The present results were obtained using Mesh B of Figure 2; and thus the finite element system involves 558 equations. The velocity vector plots and stream line contours for $Re = 1000$ and $t = 5$, 10, and 15 s are shown in Figures 14, 15, and 16, respectively. It can be seen that the present results agree with those in Reference 9 excellently, even though the present method involves less than a half of the number of equations as compared to Reference 9.

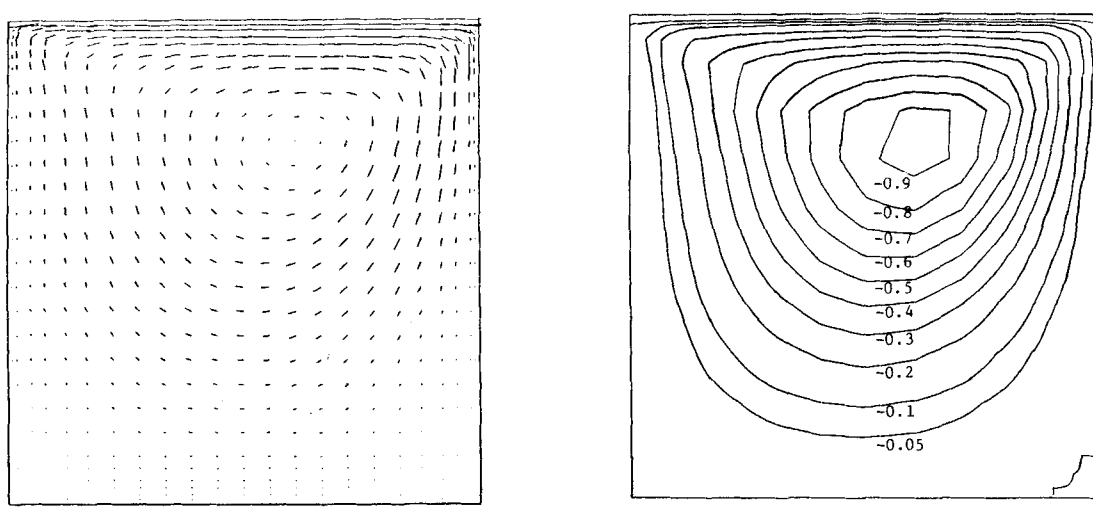

Figure 5. Driven cavity flow at $Re = 100$: (a) velocity vectors; (b) streamlines

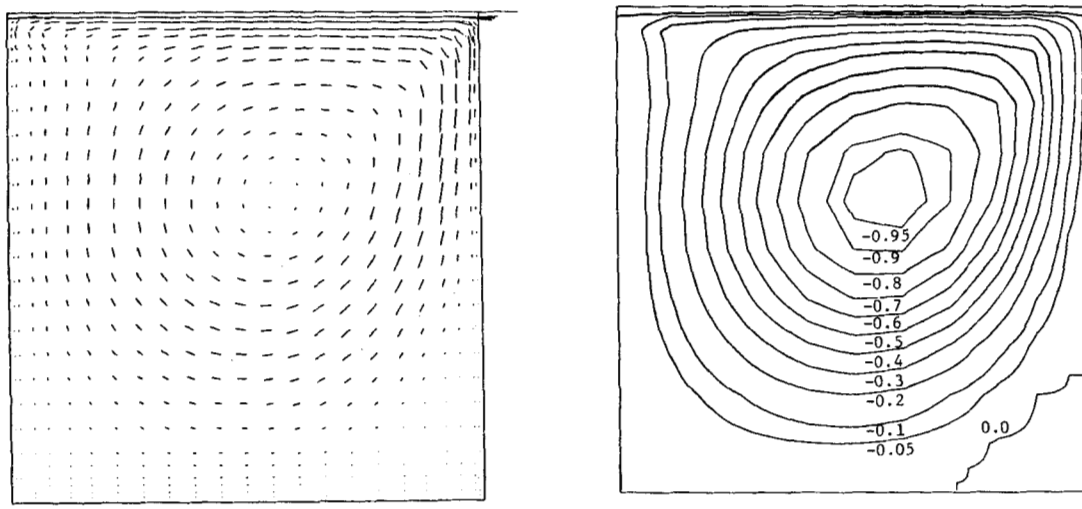

(a) (b)

Figure 6. Driven cavity flow at $Re = 400$: (a) velocity vector; (b) streamline

'JEFFRY–HAMEL' FLOW IN A CONVERGING CHANNEL

Here only the steady-state problem is considered. The problem definition is given in Figure 17.

This problem has been solved earlier by: (i) Hughes, Taylor and Levy[10] using a penalty method with bilinear velocities, and the two meshes they used lead to 110 and 460 equations, respectively. Both velocity and pressure solutions were presented for Reynolds number up to 5655; (ii) by Engelman, Strang and Bathe[11] using a penalty method with biquadratic velocities; and the mesh they used leads to 746 equations. Here, only the

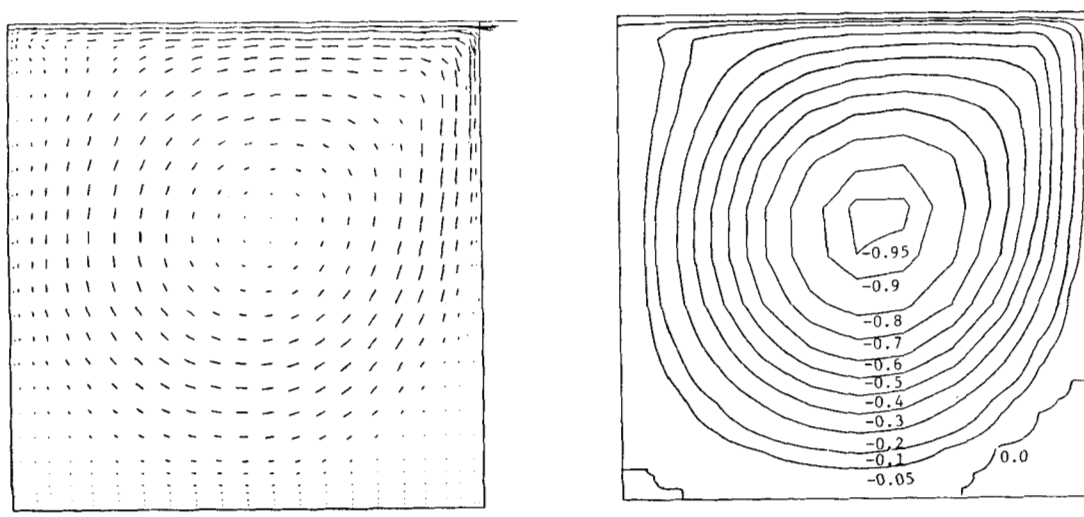

(a) (b)

Figure 7. Driven cavity Flow at $Re = 1000$: (a) velocity vector; (b) streamline

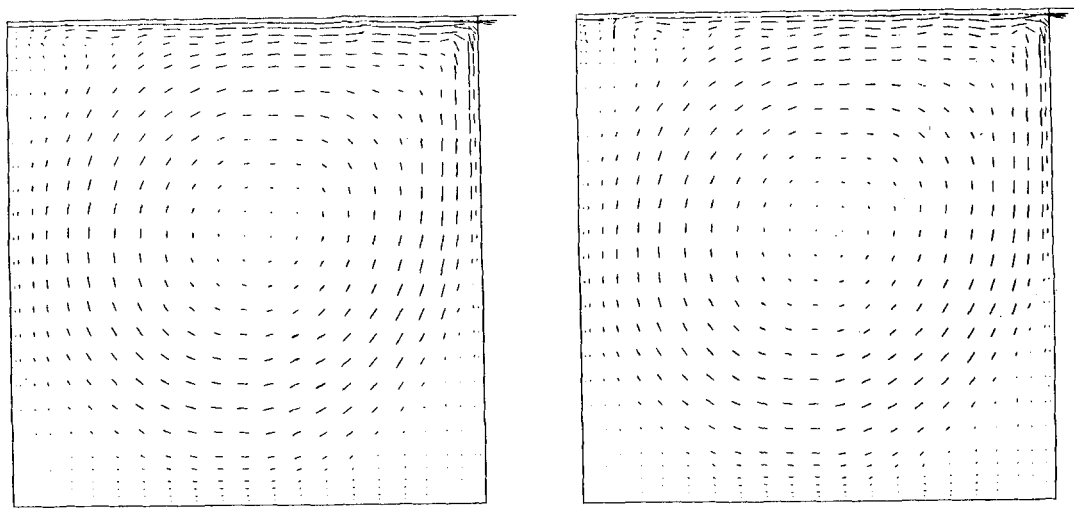

(a) (b)

Figure 8. Velocity vector plot for driven cavity flow: (a) $Re = 2000$; (b) $Re = 3000$

convergence features of the solution algorithm were presented for Re values up to 1088; (iii) Gartling, Nickell and Tanner[12] who use a primitive variable method with biquadratic velocities and bilinear pressure, with the 'best' results being obtained with a mesh resulting in 1328 equations. In Reference 12, only velocity solutions were presented for Re up to 1088; (iv) Heinrich and Marshall[3] using a penalty method with 240 biquadratic elements, but the results were presented only for velocities at $Re = 61$.

The presently employed mesh, shown in Figure 18, involves 144 four-noded elements, with a total number of equations prior to the imposition of boundary conditions being $(2 \times 169 + 144 = 482)$.

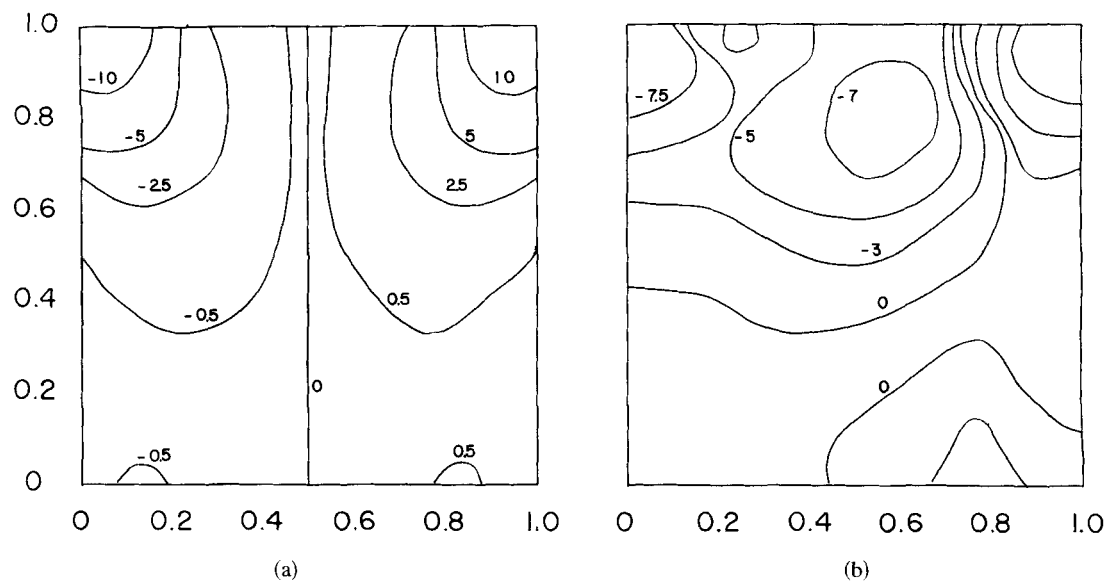

(a) (b)

Figure 9. Pressure contours for the driven cavity; (a) $Re = 0$; (b) $Re = 100$

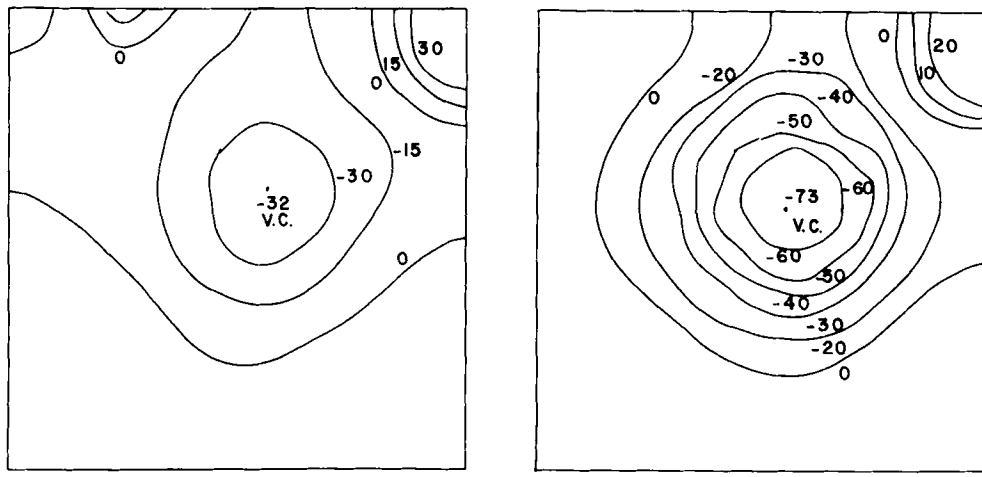

Figure 10. Pressure contours for the driven cavity: (a) $Re = 400$; (b) = 1000

The variation along the angular co-ordinate θ of the velocity in the y-direction (see Figure 18) is shown in Figure 19 for three values of $Re = 61$, 565, and 1088, respectively. Figure 20 shows the variation of velocity with radial distance along the centre line ($\theta = 0$) for two values of $Re = 61$ and 1088, respectively. Figure 21 shows the variation with θ of the quantity $(v_r \cdot r)$ (v_r is the radial velocity) at $r = 1$, for three values of $Re = 61$, 565, and 1088, respectively. Figure 22 shows the variation with θ at radial locations $r = 1{\cdot}0$ and $2{\cdot}2$, respectively, as well as the variation with r at θ locations $\theta = 4{\cdot}3°$ and $29{\cdot}3°$, respectively, of the pressure field at $Re = 565$. Finally, the normalized radial velocity profiles at $Re = 565$ are shown as functions of θ for two values $r = 1{\cdot}0$ and $r = 2{\cdot}2$, respectively, in Figure 23.

The present results can be seen to be in excellent agreement with the results reported in References 10–12 and 3 as well as the analytical results.[13]

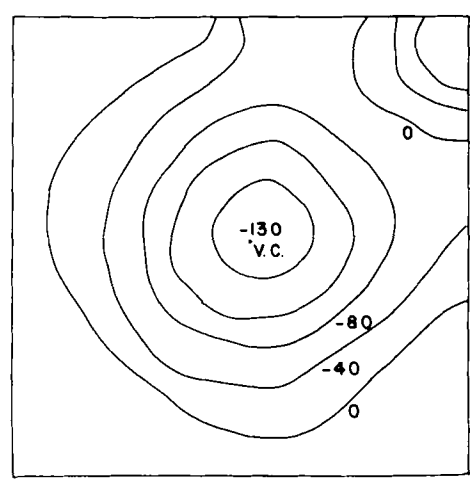

Figure 11. Pressure contours for the driven cavity: $Re = 3000$

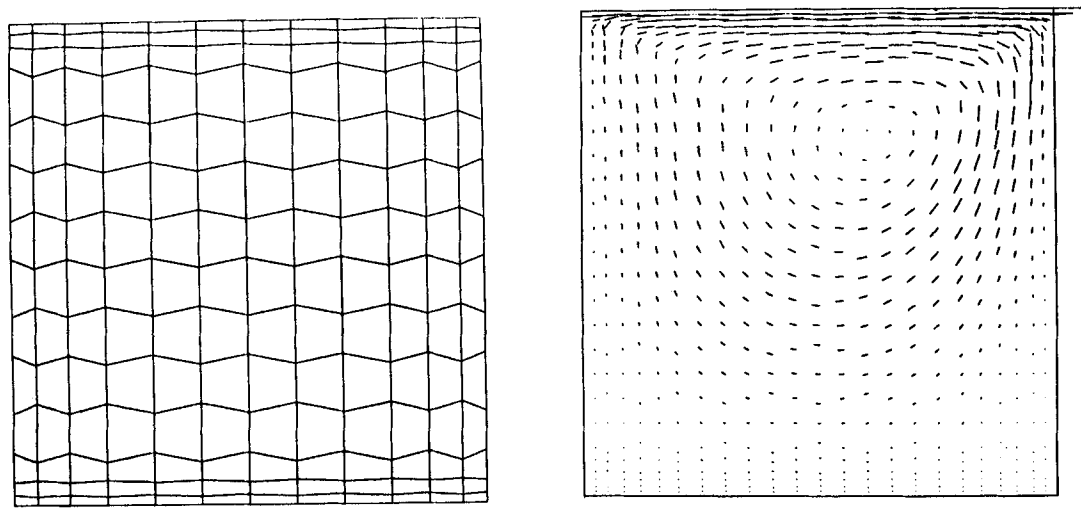

(a) (b)

Figure 12(a). Distorted finite element mesh for driven cavity flow: Number of elements = 168; Number of points = 195: (b) Velocity vector plot ($Re = 100$) for distorted mesh

FLOW OVER A 'BACKWARD' OR 'DOWNSTREAM' FACING STEP

The problem definition is given in Figure 24, which shows a backward facing step of expansion ratio (2:3). At the top as well as bottom walls, the boundary conditions are $v_x = v_y = 0{\cdot}0$. At the inlet the boundary conditions are $v_y = 0$ and $v_x = 4y(1-y)$ with the origin of y as shown in Figure 24. Two different types of outlet conditions are used: (i) traction free conditions $t_x = t_y = 0$; (ii) $v_y = 0$, and $t_x = 0$.

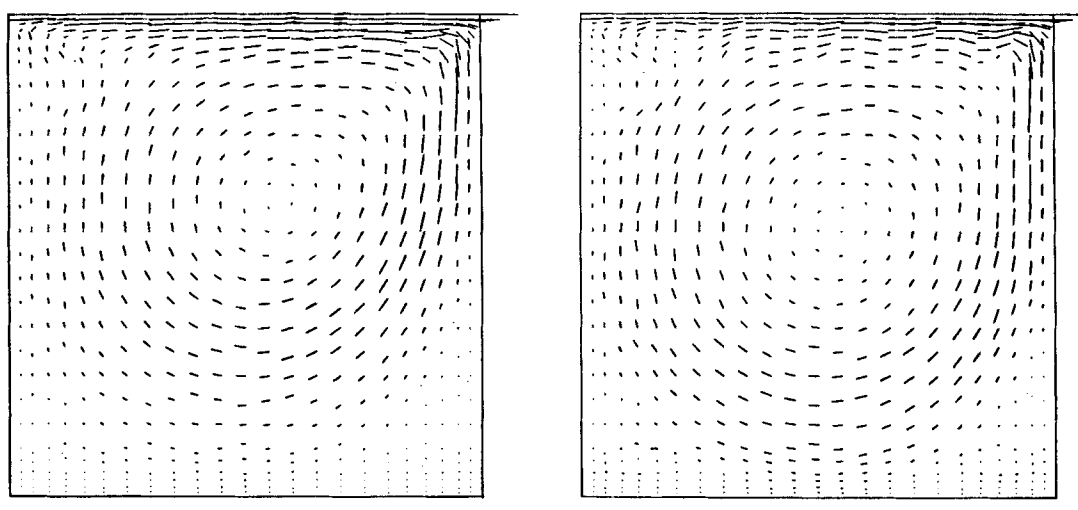

(a) (b)

Figure 13(a). Velocity vector plot ($Re = 400$) for distorted mesh: (b) Velocity vector plot ($Re = 1000$) for distorted mesh.

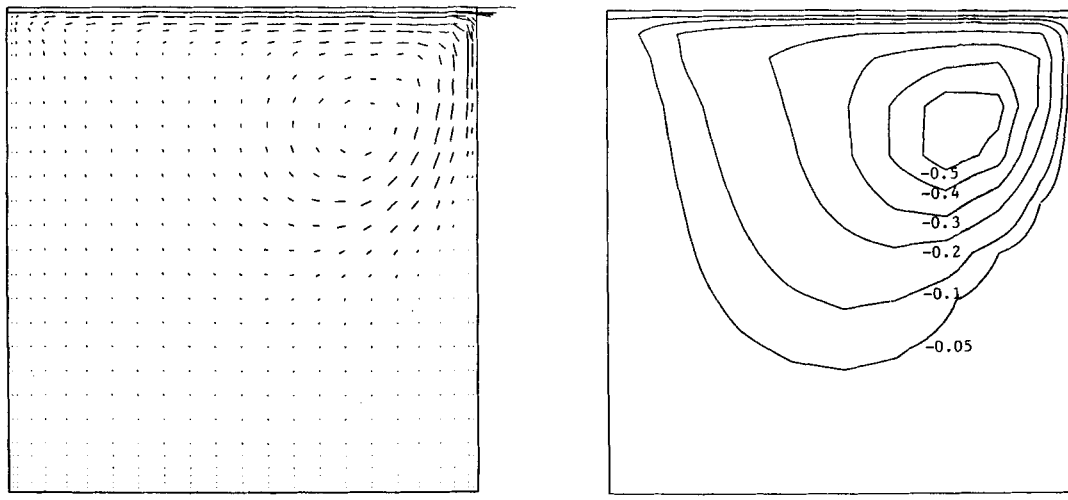

(a) (b)

Figure 14. Driven cavity flow at $t = 5$ s: (a) velocity vectors; (b) streamlines

Experimental work on this problem has been reported by Denham and Partick.[14] Finite difference calculations using 'upwind' difference schemes were reported by Atkins, Maskell and Patrick.[15] In Reference 15 it was found that the upwind difference scheme underestimates the length as well as the intensity of the recirculation zone as compared to the conventional conditionally stable central difference method. Finally a finite element analysis of this problem was presented recently by Thomas, Morgan and Taylor[16] who employed a 'velocity–pressure' formulation. The convection term was treated in Reference 16 by using the conventional Galerkin technique as well as the 'upwinding' technique. In Reference 16, eight-noded elements with quadratic velocity fields and linear pressure fields were used.

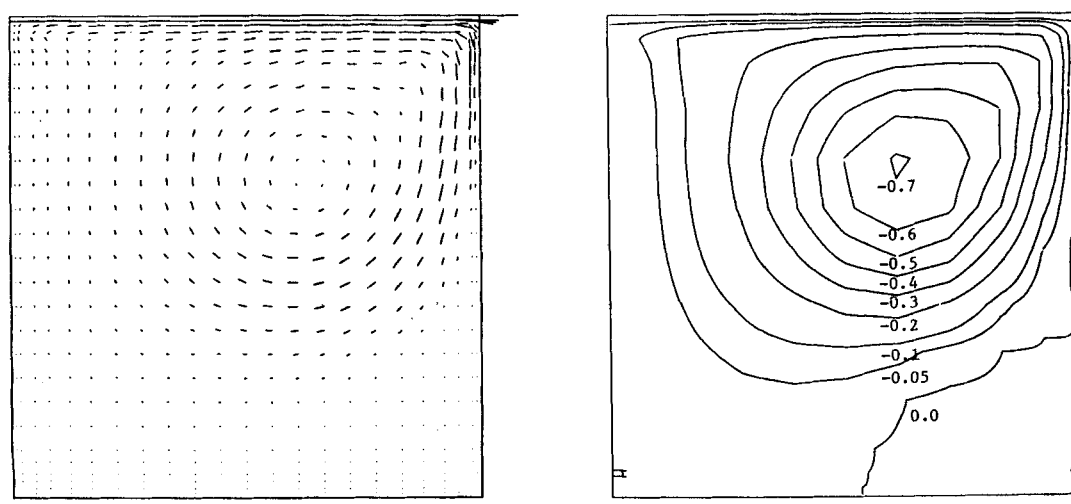

(a) (b)

Figure 15. Driven cavity flow at $t = 10$ s: (a) velocity vectors; (b) streamlines

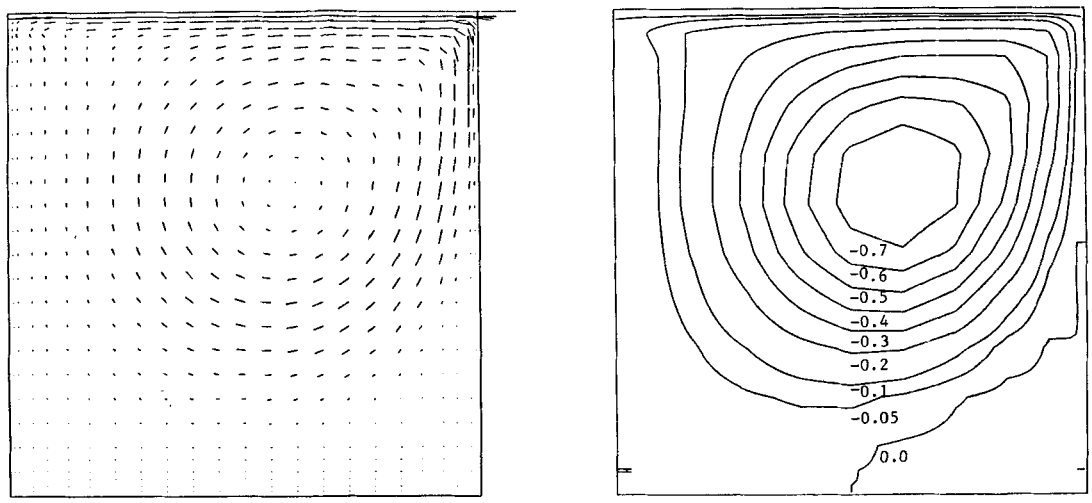

Figure 16. Driven cavity flow at $t = 15$ s: (a) velocity vectors; (b) streamlines

The results for velocities and stream-functions presented in Reference 16 correspond to a finite element mesh (Figure 8 of Reference 16) with: (i) the inlet length (prior to expansion) of 3 units (ii) the outlet length (after expansion) of 22 units, and (iii) total equations (velocity and pressure) of about 520. The authors of Reference 16 state that for this mesh: (i) they could not obtain convergence for $Re \geq 100$ when the outlet boundary conditions were $t_x = 0$ and $v_y = 0$; (ii) convergence for $Re \geq 100$ was obtained when the outlet boundary condition was changed to $t_x = 0$ and $t_y = 0$, and in addition a condition that $v_y = 0$ was imposed at the first node down stream of the step and at the same level (see Figure 2 of Reference 16); (iii) 'upwinding' was necessary to obtain reasonable converged results at $Re = 125$ even with the boundary condition as in (ii), whereas even 'upwinding' resulted in failure of convergence at $Re = 125$ when the outlet conditions were $t_x = 0$ and $v_y = 0$. However, even though the results did not converge for $Re = 125$, $t_x = 0$, $v_y = 0$, it appears that 'upwinding' stabilized and smoothed out the results. It should also be remarked that in Reference 16 results *failed*

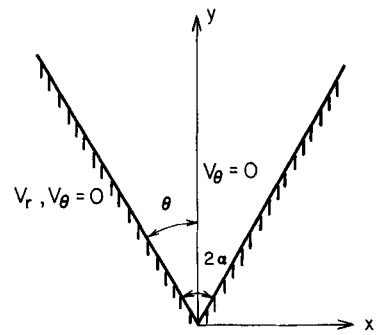

Figure 17. Problem definition for Jeffry–Hamel flow: $\alpha = \pi/6$; $Re = \rho\alpha\,|V(r, 0)|\, r/\mu = \rho\pi/6$ (take μ unit). For numerical solution, the range $1/4 \leq r \leq 4$ and $0 \leq \theta \leq \pi/6$ is modelled. Boundary conditions are (i) traction free at $r = 1/4$; (ii) $V_r = V_\theta = 0$ along $\theta = \pi/6$; (iii) $V_\theta = 0$ along $\theta = 0$; (iv) $V_\theta(r, \theta) = 0$ at $r = 4$ and two different $V_r(r, \theta)$ at $r = 4$: (1) $V_r(r, 0)r = 1$; (2) $V_r(r, 0)r = 4$

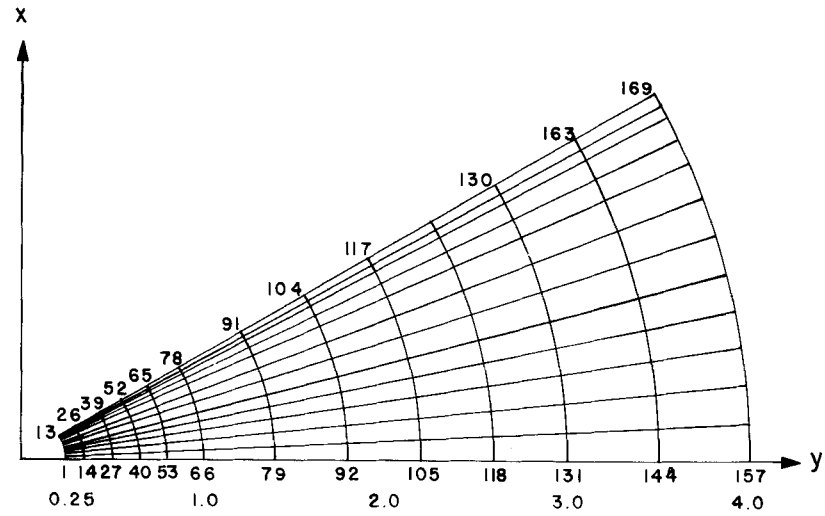

Figure 18. Finite element mesh for Hamel flow: Total number of elements = 144. Total number of nodes = 169

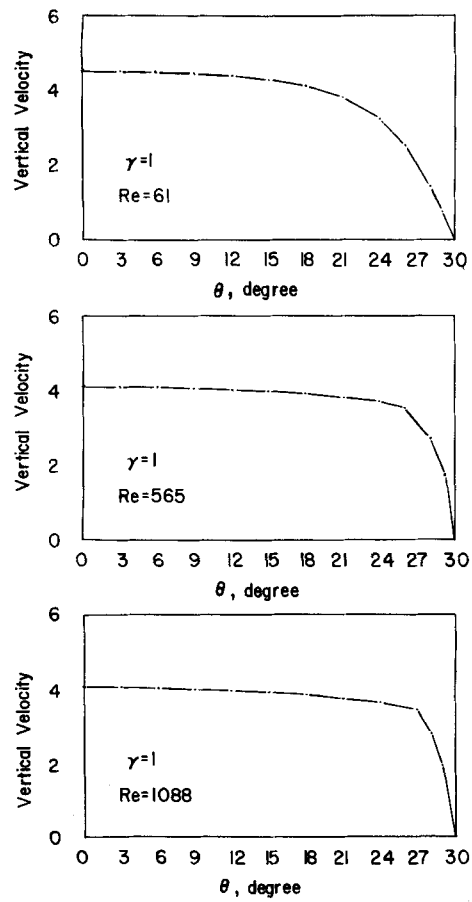

Figure 19. Vertical velocity vs angle (at $r = 1$) for different Re numbers

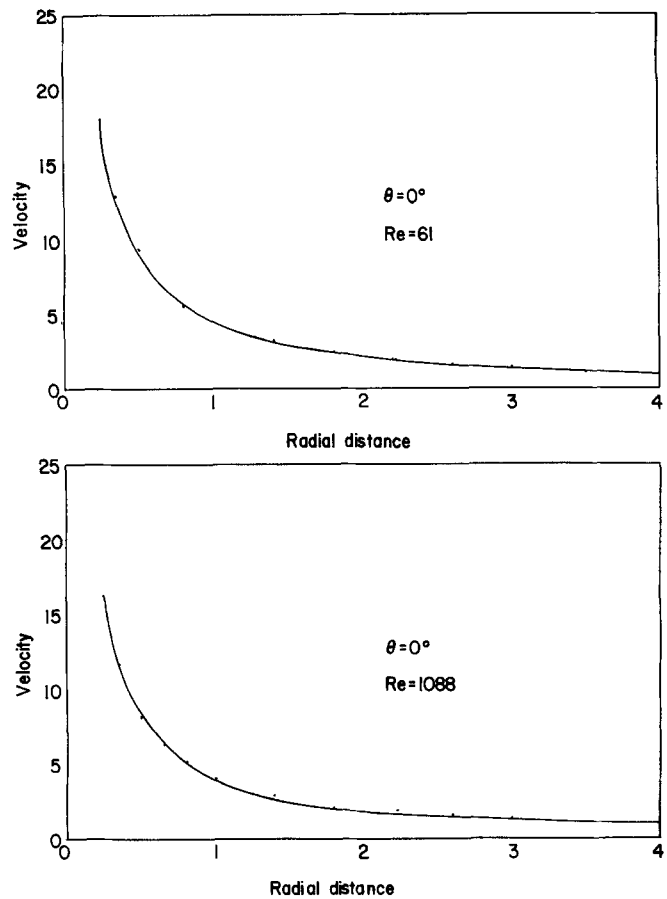

Figure 20. Centre line velocity vs. radius

to converge for $Re \geq 73$ when: (i) the inlet length (prior to expansion) was 6·5 units and (ii) the outlet length (after expansion) was 12 units.

In contrast, in the present set of results, the following apply: (i) the inlet length is 2 units, (ii) the outlet length is 8 units, (iii) the inlet conditions are $v_x = 4y(1-y)$, and $v_y = 0$; (iv) the results are presented for *both* sets of outlet conditions ($t_x = 0$, $v_y = 0$) as well as ($t_x = t_y = 0$), and *Re* values of 73, 125, 191, and 229 respectively.

Based on the studies of Leone and Gresho[17] (see Figure 5 therein) it may be surmised that the inlet length has no noticeable effect on the obtained solution. However, the results of Reference 17 do indicate that the longer the outlet length, the smoother and more stable the solutions are. Further, the numerical experiments of Reference 17 tend to suggest that traction-free conditions at the outlet result in better, smoother, and more stable solutions. Even though the studies in Reference 17 are for a flow in a channel past a rectangular obstacle, the effect of outlet conditions can be seen to be similar to the present problem of flow past a backward facing step. Thus the above comments should be kept in mind while comparing the present results with those of Reference 16.

The finite element mesh used in the present computations is shown in Figure 25; it consists of 172 four-noded elements with a total number of $(2 \times 201 + 172) = 574$ equations prior to

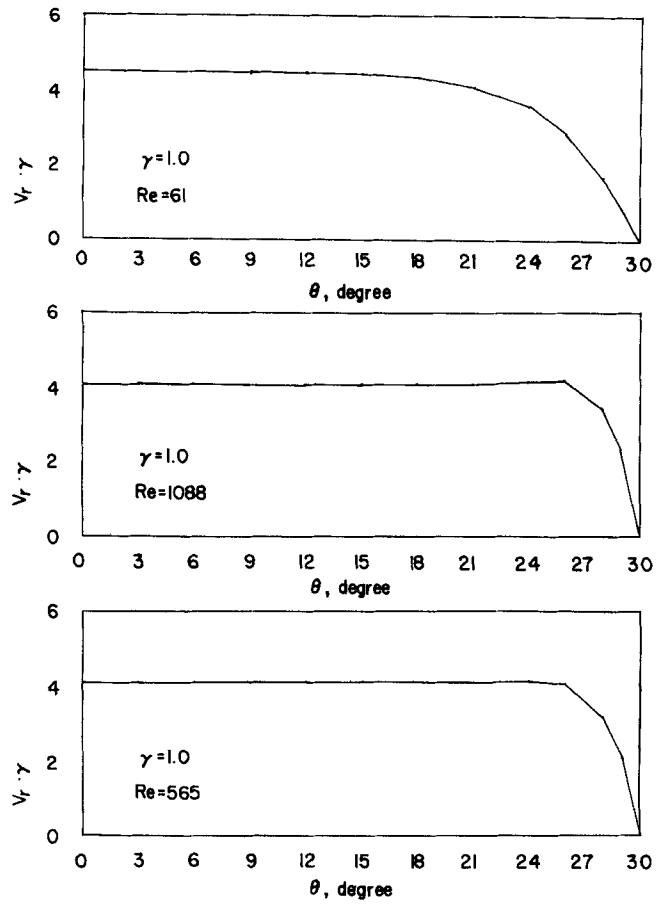

Figure 21. Variation of $(V_r \times r)$ with θ for different Re numbers

the imposition of boundary conditions. Figure 26 shows the velocity vector plots as well as the stream lines for $Re = 73$ and the outlet b.c. of $t_x = t_y = 0$. Likewise Figures 27, 28, 29, and 30 show the velocity vector plots as well as the stream lines for $Re = 125$, 155, 191 and 229, respectively, and for outlet b.c. $t_x = t_y = 0$. Note that in all these computations, as stated in Part I of this paper, no 'upwinding' was used. More interestingly, Figures 31, 32, and 33 show, respectively, the velocity vector plots an stream line contours for $Re = 125$, 155, and 191 and for outlet b.c. $t_x = v_y = 0$. These results are rather 'smooth', *even for the present outlet length of* 8 *units.*

Finally, in Figure 34, the presently computed lengths of the recirculation zones, as well as those from References 15 and 16, are compared with the experimental results of Reference 14. It should be borne in mind, however, that the inlet condition for $v_x = 4y(1-y)$ in the present calculation as well as those in References 15 and 16, but this may be different from the experimental inlet condition. Also References 15 and 16 use upwinding schemes, while the present method uses a conventional Galerkin technique. From Figure 34 it is evident that the present results are in best agreement with the experimental measurements.

We believe that the above results effectively serve to illustrate the accuracy and efficiency of the present approach.

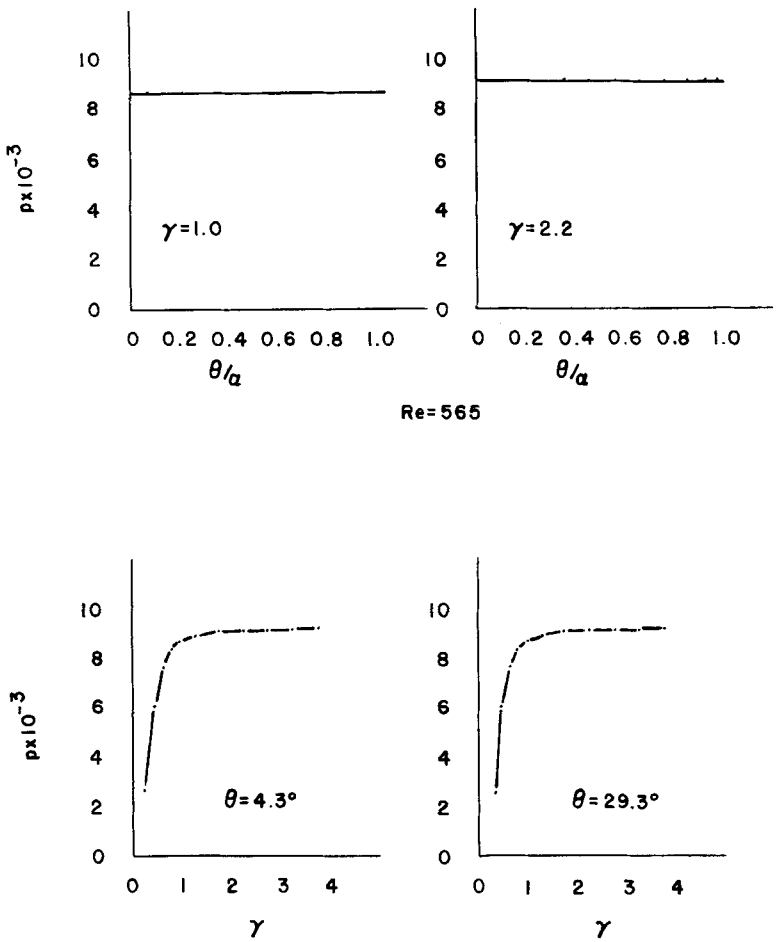

Figure 22. Circumferential and radial pressure profiles, $Re = 565$ ($V_\gamma(\gamma, 0)\gamma = 1$ at $\gamma = 4$)

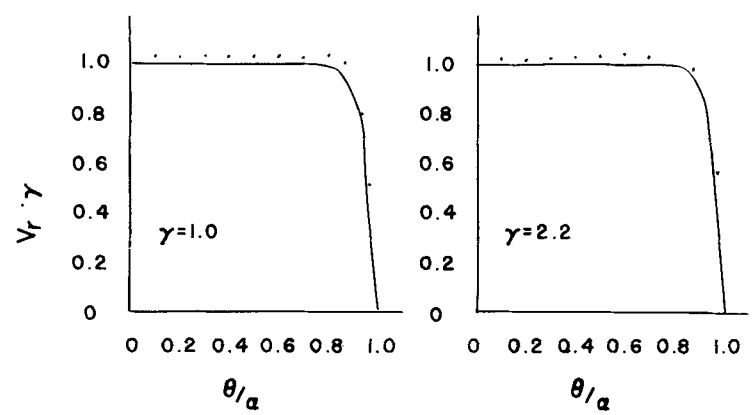

Figure 23. Normalized radial velocity profiles, $Re = 565$ ($V_\gamma(\gamma, 0)\gamma = 1$ at $\gamma = 4$)

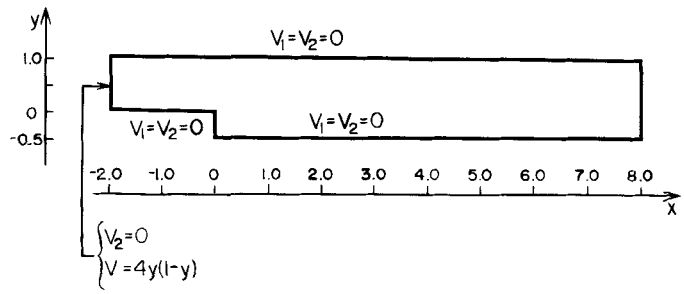

Figure 24. Problem definition for flow over a backward facing step: Boundary conditions (i) Parabolic inlet profile at $x = -2{\cdot}0$, i.e. $V_1 = 4y(1-y)$, $V_2 = 0$; (ii) Two different outlet boundary conditions at $x = 8{\cdot}0$; (1) traction free; (2) $V_2 = 0$

Figure 25. Finite element mesh for flow over a backward facing step: Number of elements = 172; Number of points = 201

FLOW OVER A SQUARE STEP

The problem definition is given in Figure 35. It is to be remarked that this is the problem that led Hughes, Liu and Brooks[1] to believe that the Gauss–Legendre integration of the convection term is inappropriate, and to suggest an 'upwinding' treatment. This conclusion in Reference 1 has later been a subject of intense scrutiny by Leone and Gresho.[17] In the following we discuss the results for this problem, obtained through the present approach, for both steady and unsteady cases.

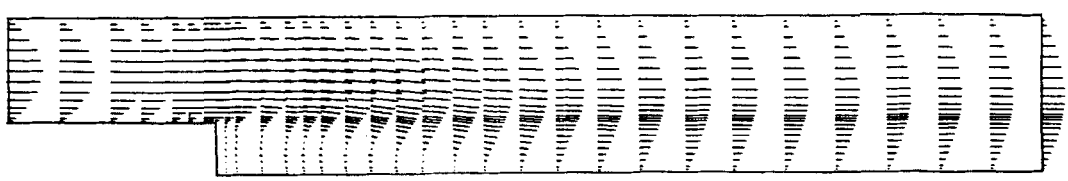

(a)

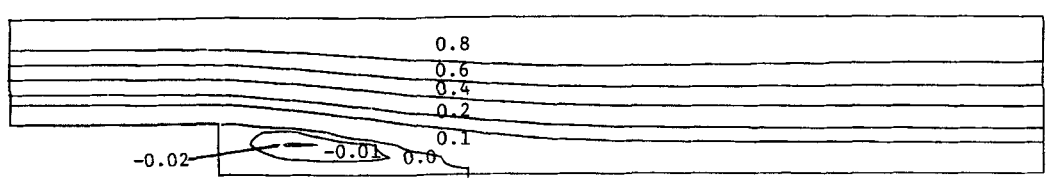

(b)

Figure 26. Flow over a backward facing step with traction free outlet b.c. at $Re = 73$: (a) velocity vectors; (b) streamlines, (numerical values are of dimensionless stream function ψ/ψ_{max})

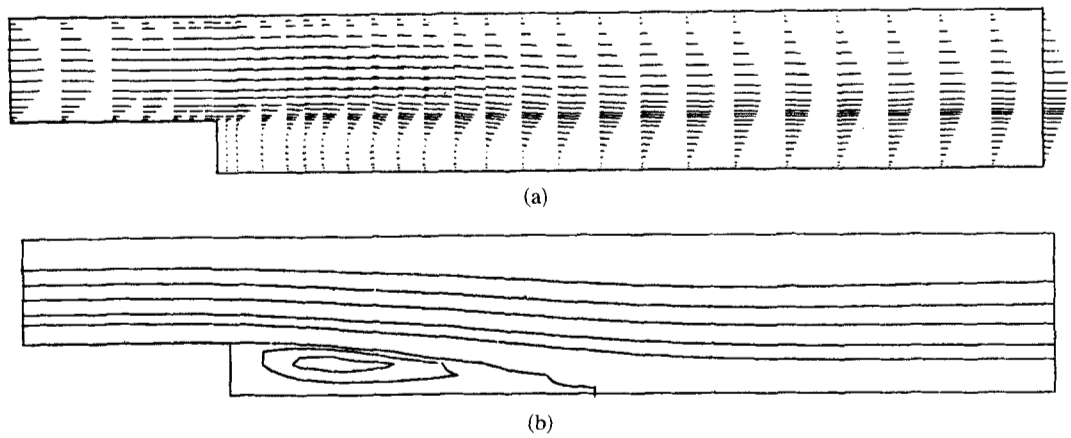

(a)

(b)

Figure 27. Flow over a backward facing step with traction free outlet b.c. at $Re = 125$: (a) velocity vectors; (b) streamlines

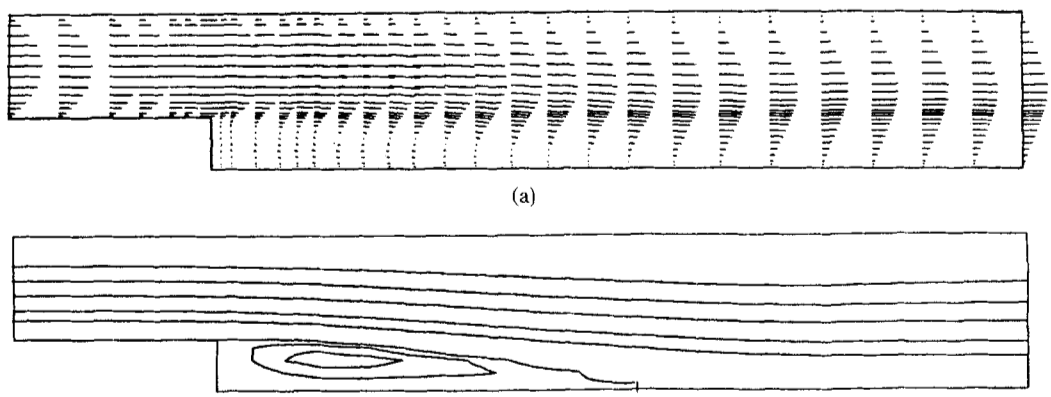

(a)

(b)

Figure 28. Flow over a backward facing step with traction free outlet b.c. at $Re = 155$: (a) velocity vectors; (b) streamlines

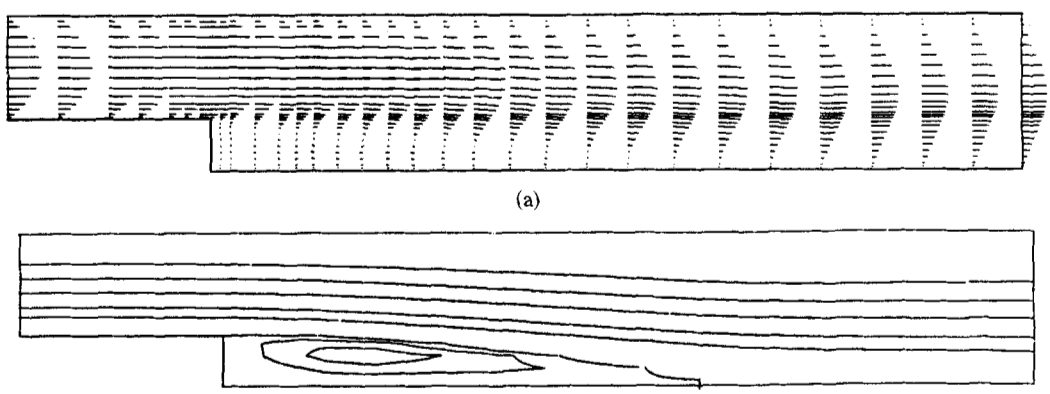

(a)

(b)

Figure 29. Flow over a backward facing step with traction free outlet b.c. at $Re = 191$: (a) velocity vectors; (b) streamlines

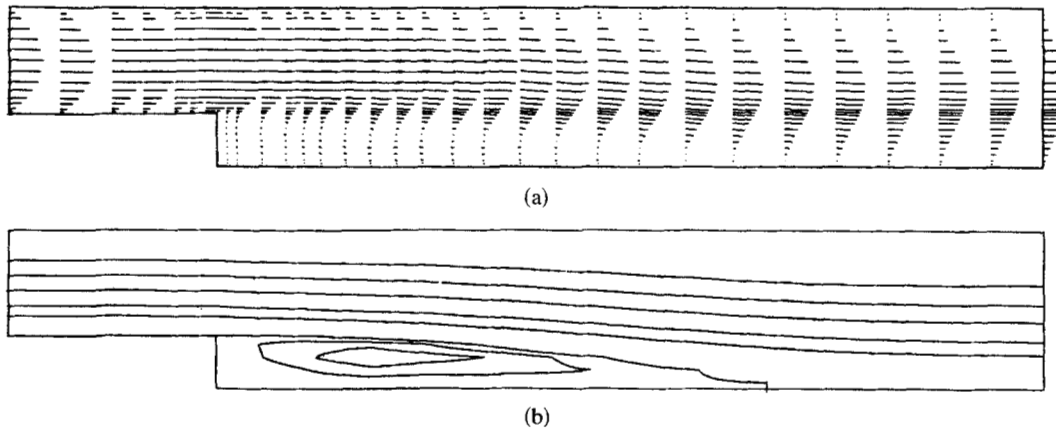

(a)

(b)

Figure 30. Flow over a backward facing step with traction free outlet b.c. at $Re = 229$: (a) velocity vectors; (b) streamlines

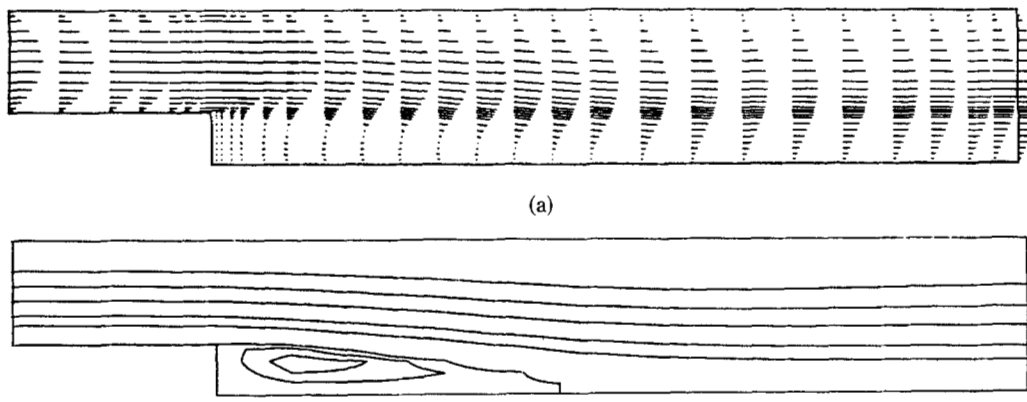

(a)

(b)

Figure 31. Flow over a backward facing step with outlet b.c. of $V_2 = 0$; $Re = 125$: (a) velocity vectors; (b) streamlines

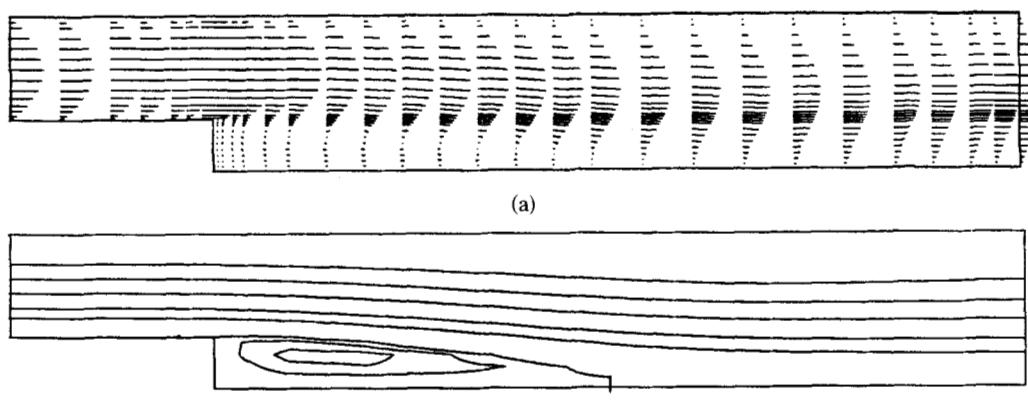

(a)

(b)

Figure 32. Flow over a backward facing step with outlet b.c. of $V_2 = 0$; $Re = 155$: (a) velocity vectors; (b) streamlines

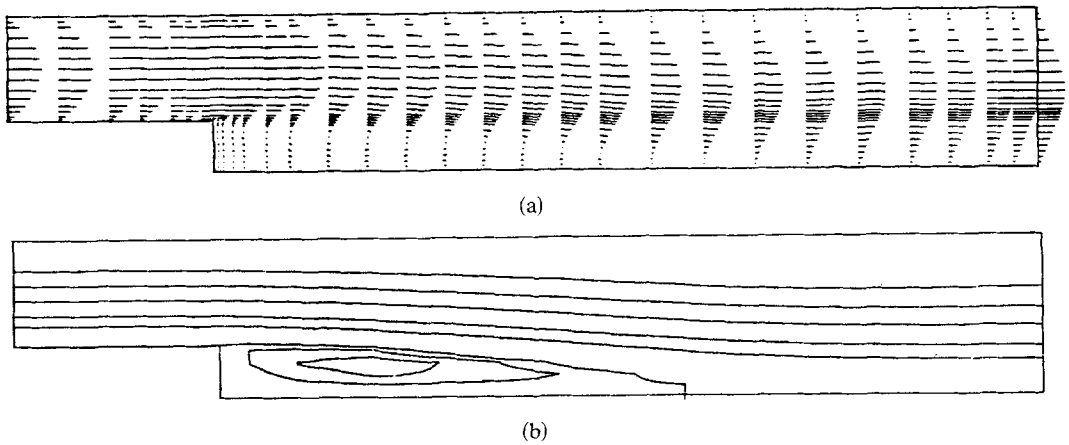

Figure 33. Flow over a backward facing step with outlet b.c. of $V_2 = 0$; $Re = 191$: (a) velocity vectors; (b) streamlines

(a) *Steady flow*

Following Hughes, Liu and Brooks[1] and Leone and Gresho[17] we consider flow in a 1 unit high channel consisting of a step located at 1·2 units from the inlet which is 0·4 units high and 0·4 units across. The inlet boundary condition is $v_x = 1$, $v_y = 0$. The outlet boundary conditions are $t_x = t_y = 0$. Following Leone and Gresho,[17] two cases of outlet location are considered: 4 units and 6 units from the inlet, respectively.

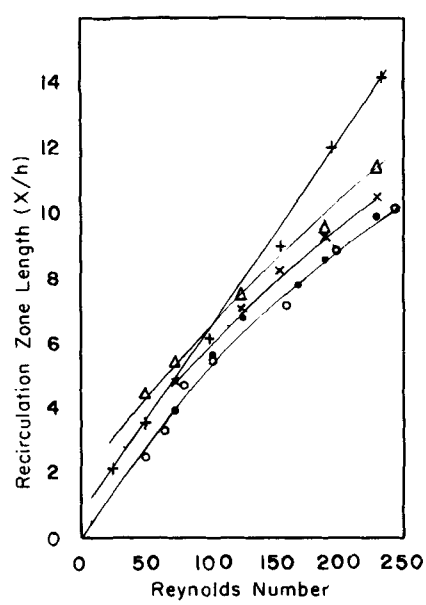

Figure 34. Length of recirculation zone vs Re number: × Present mixed FEM; △ FEM with upwinding[16] + FDM (by Atkins *et al.*)[15]

● Laser anemometes
○ Dye-tracer
} Experimental result[14]

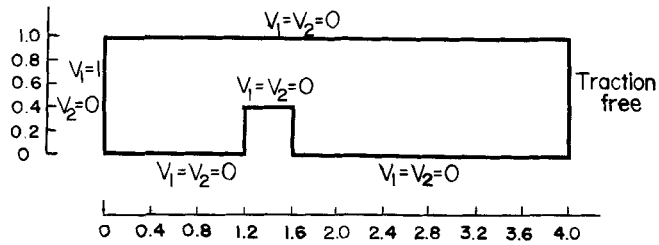

Figure 35. Problem definition for flow over a square step

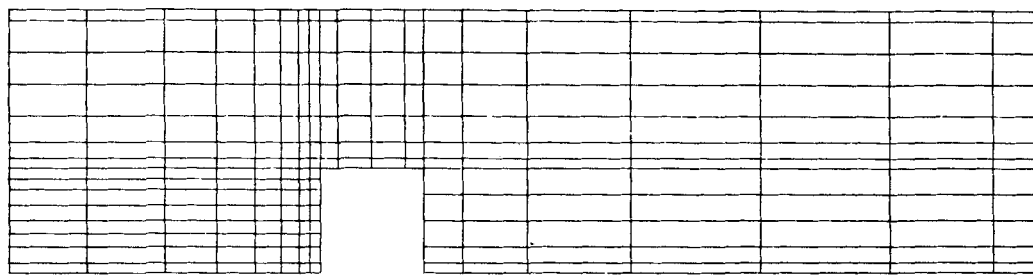

Figure 36. Finite element mesh (I) for flow over a square step; Total number of elements = 232; Total number of points = 272

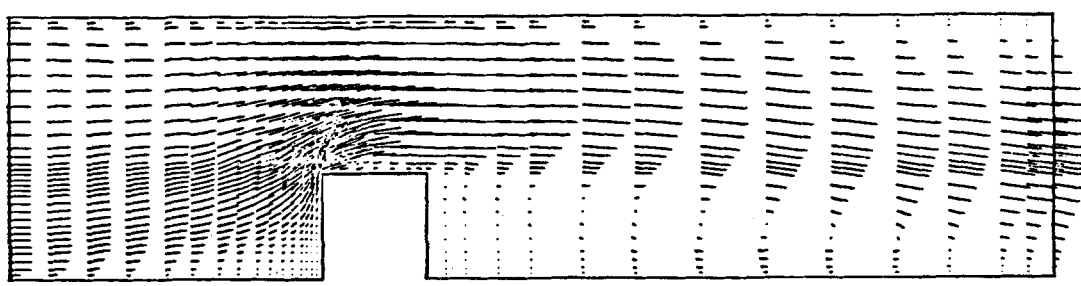

(a)

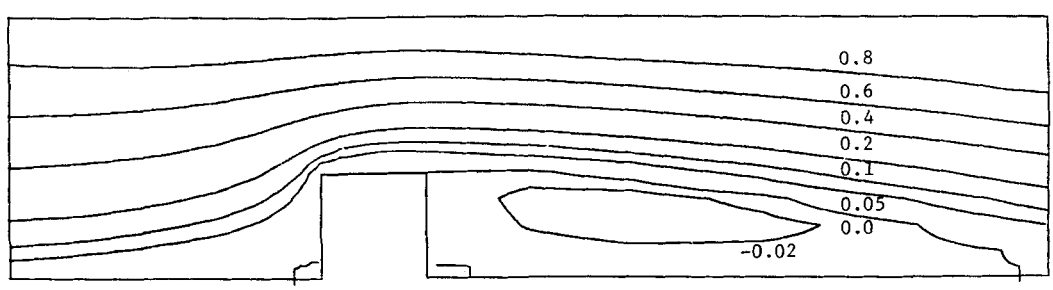

(b)

Figure 37. Flow over a square step, $Re = 200$, mesh (I): (a) velocity vectors; (b) streamlines

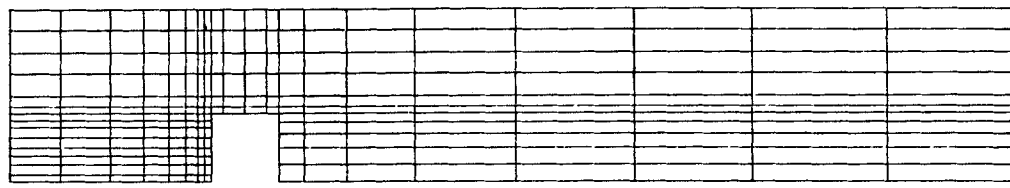

Figure 38. Finite element mesh (II) (extended version of mesh (I)): Total number of elements = 224; Total number of points = 264

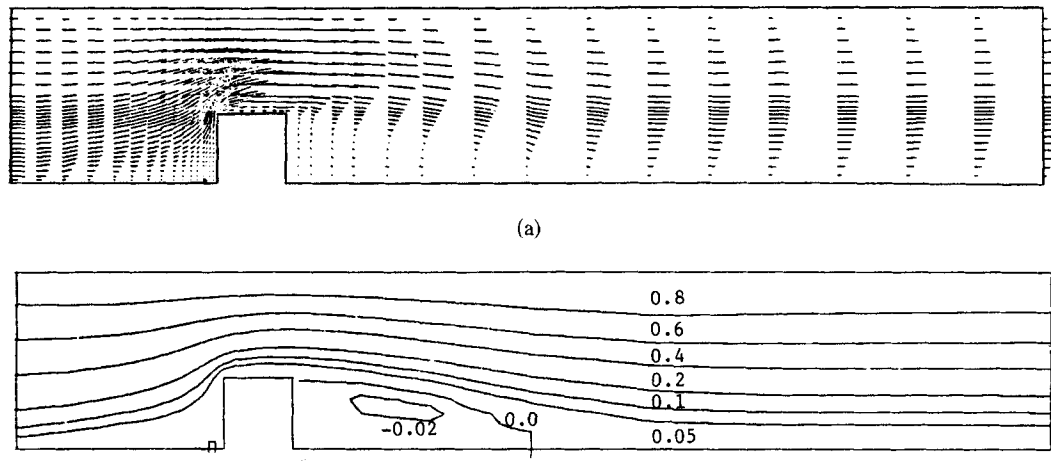

(a)

(b)

Figure 39. Flow over a square step at $Re = 85$, mesh (II): (a) velocity vector; (b) streamline

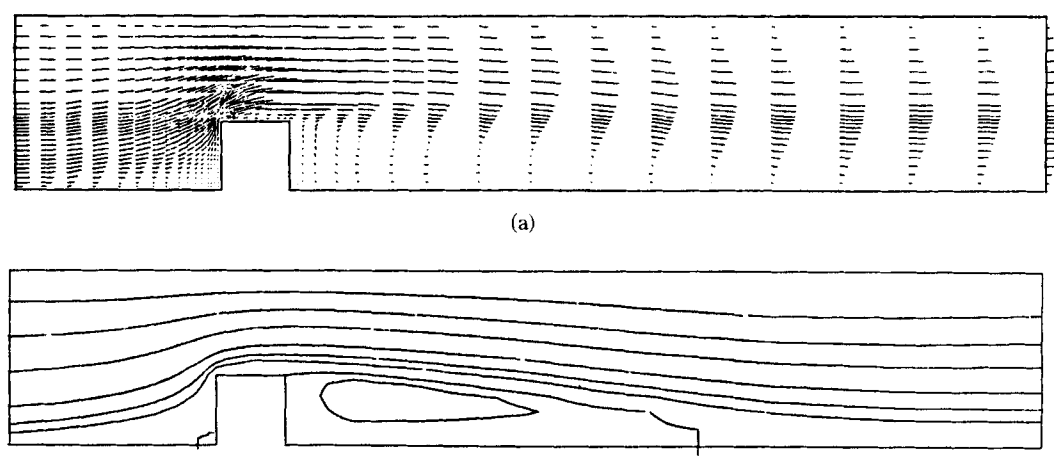

(a)

(b)

Figure 40. Flow over a square step, $Re = 200$, Mesh (II): (a) velocity vector; (b) streamline

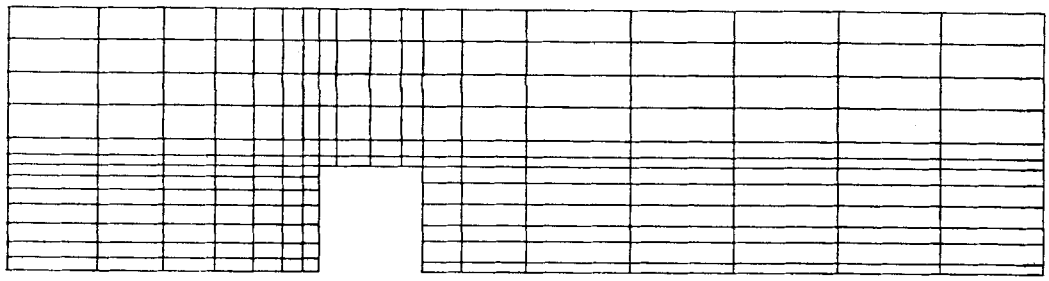

Figure 41. Finite element mesh, $Re = 85$, channel length = 4 units; Number of elements = 199; Number of points = 237; Number of d.o.f. = 673

Leone and Gresho[17] studied this problem exhaustively using a velocity–pressure formulation and conventional Galerkin technique, wherein a 9 noded element with biquadratic velocities and bilinear approximation for pressure is used.

The presently used mesh, when the considered length of channel is 4 units is shown in Figure 36. It consists of 232 four-noded elements with constant pressure, with 272 nodes, and the total number of equations are $(2\times272+232)=776$ prior to the imposition of the boundary conditions. This is to be contrasted with Grid 2 of Leone and Gresho (Figure 16 of Reference 17) which consists of 155 nine-noded elements with 1558 equations, presumably prior to the imposition of boundary conditions. Thus the present method involves roughly half the number of equations compared to Reference 17. For this length of the channel, the computed velocity vectors and the stream line plots at $Re = 200$ are shown in Figure 37. It should be noted that for this channel length, the results of Reference 17 show a spurious second eddy near the outlet, which as such is absent in the present Figure 37. It should also

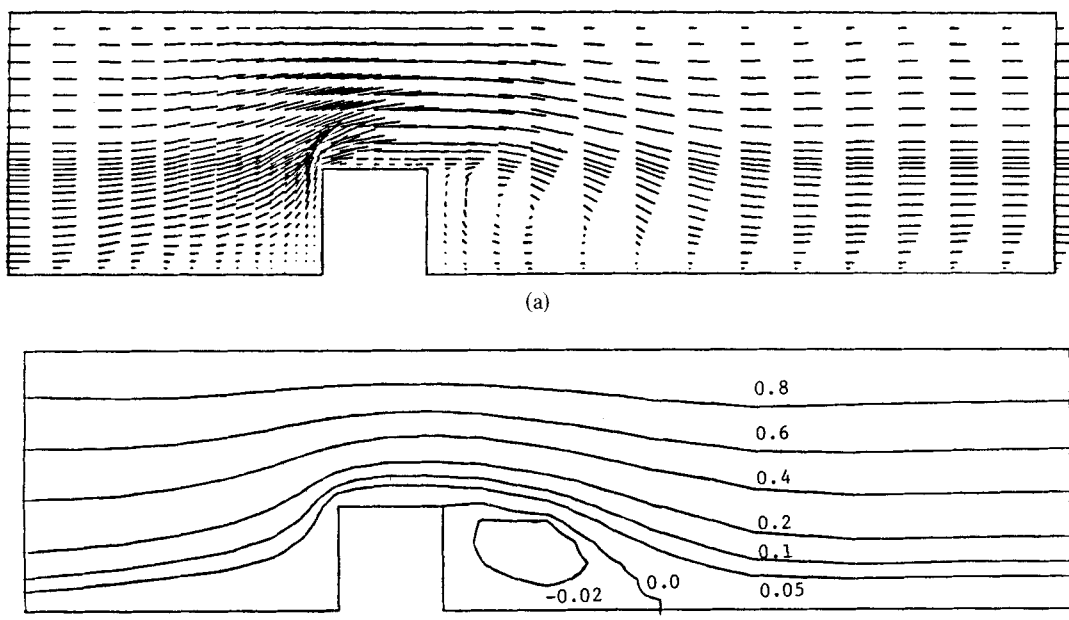

(a)

(b)

Figure 42. Unsteady flow, $Re = 85$, $t = 1.0$ s; (a) velocity vectors; (b) streamlines

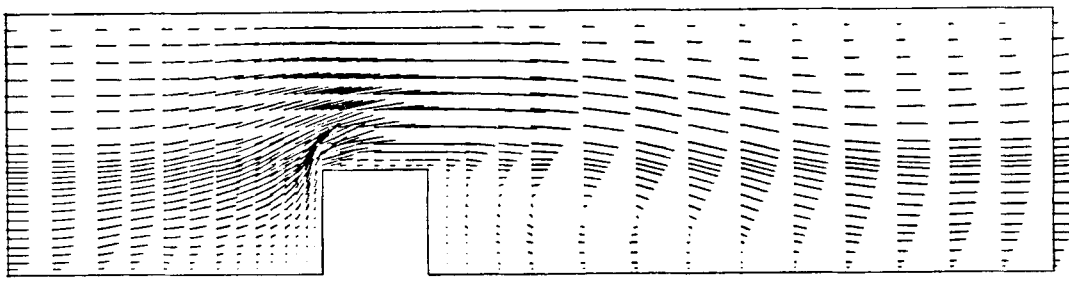

(a)

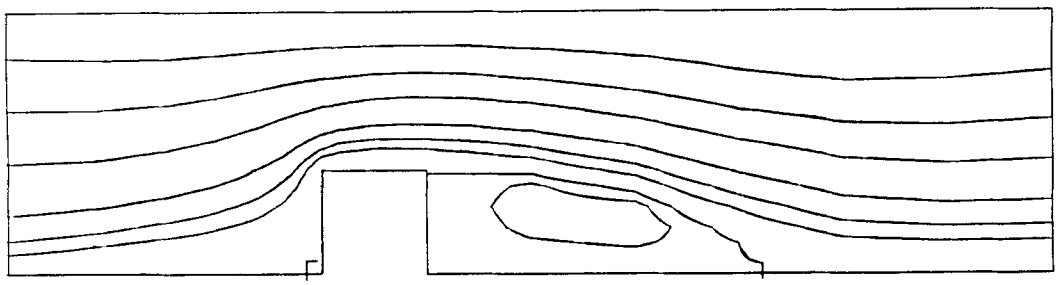

(b)

Figure 43. Unsteady flow at $Re = 85$, $t = 2{\cdot}0$ s; (a) velocity vectors; (b) streamlines

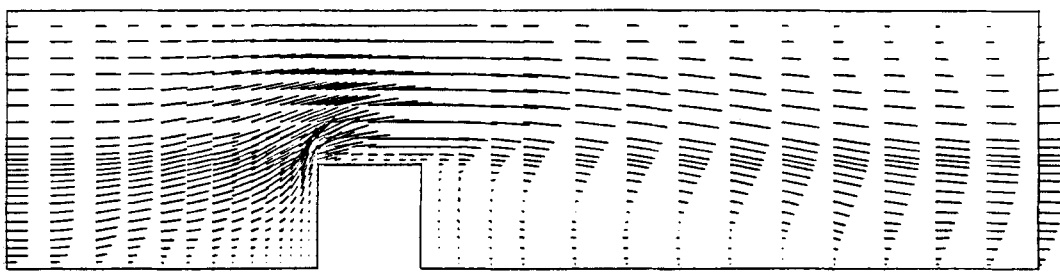

(a)

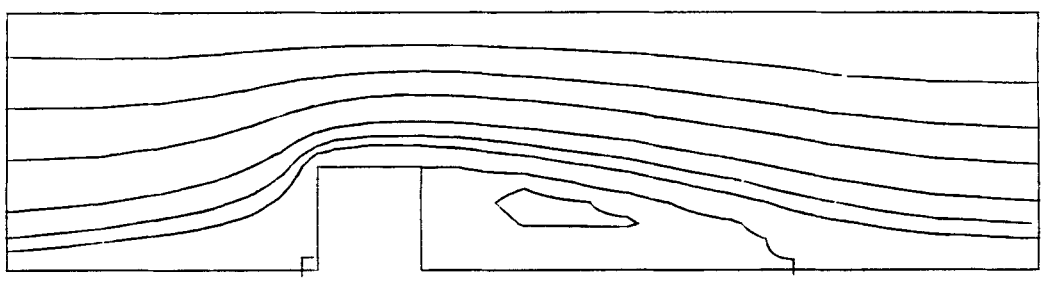

(b)

Figure 44. Unsteady flow at $Re = 85$, $t = 3{\cdot}0$ s: (a) velocity vectors; (b) streamlines

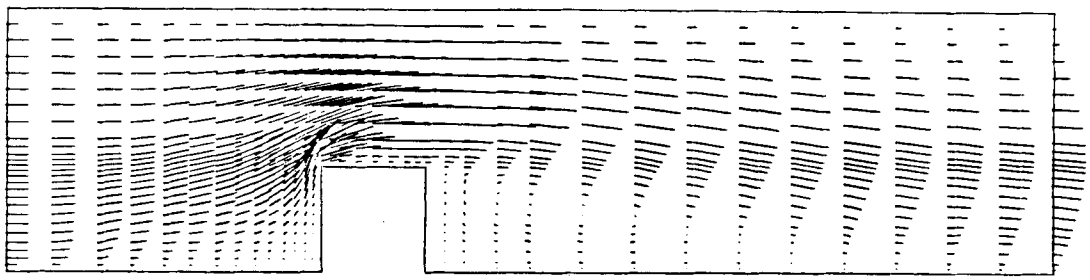

(a)

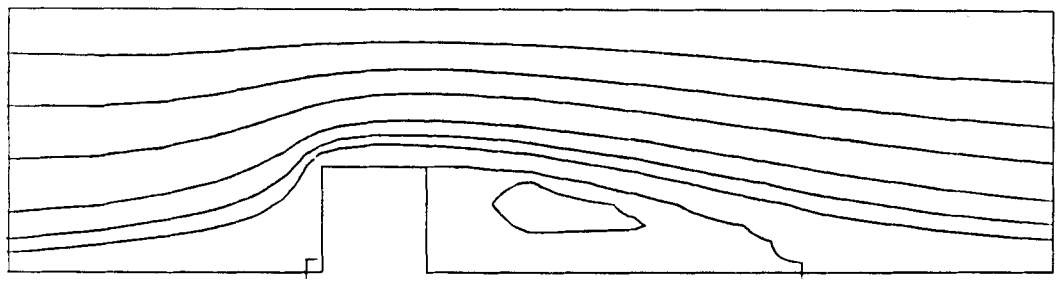

(b)

Figure 45. Unsteady flow at $Re = 85$, $t = 4{\cdot}0$ s: (a) velocity vectors; (b) streamlines

be remarked that the length of the eddy shown in Figure 37 is comparable to that found by Leone and Gresho[17] for the case when the channel length is 6 units.

The finite element mesh used in the present computation, when the channel length is 6 units is shown in Figure 38. It consists of 224 four-noded elements with constant pressure, with 264 nodes, and the total number of equations is $(2\times 264+224)=752$ prior to the imposition of the boundary consditions. This should be contrasted with Grid 3 of Leone and Gresho (Figure 1(c) of Reference 17) which consists of 205 nine-noded elements with 2033 equations, presumably prior to the imposition of the boundary conditions. For this channel-length case, the computed velocity vector plots and stream line contours for $Re = 85$ are shown in Figure 39, whereas similar results are shown in Figure 40 for $Re = 200$. The results for both $Re = 200$ and 85 are found to be in excellent agreement with those of Leone and Gresho.[17] Based on a comparison of the eddy length, Leone and Gresho[17] concluded that eventhough the same problem was solved by Hughes, Liu and Brooks[1] for $Re = 200$ using 'upwinding', the *effective* Re in the upwinding similation[1] to be 85. The present results for $Re = 85$ (which are in excellent agreement with those of Reference 17) appear to confirm this conclusion.

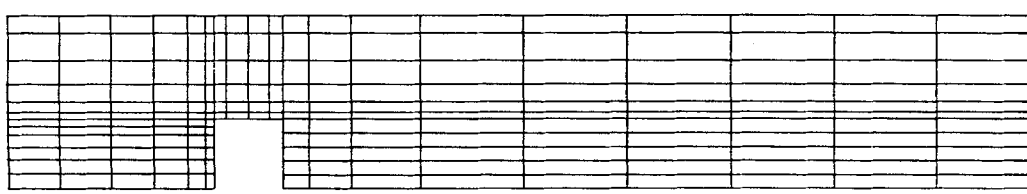

Figure 46. Mesh for analysis of unsteady flow at $Re = 200$: Total number of elements = 195; Total number of points = 232

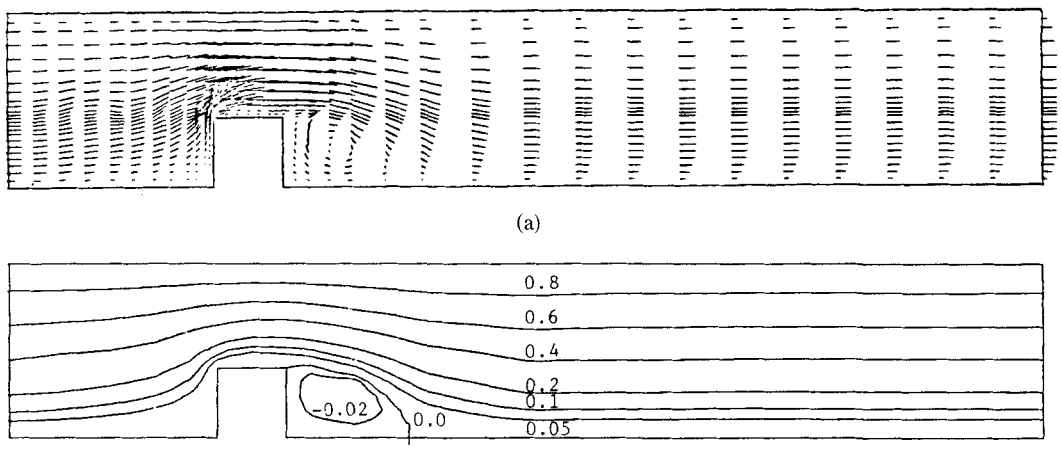

(a)

(b)

Figure 47. Unsteady flow at $Re = 200$, $t = 1{\cdot}0$ s: (a) velocity vectors; (b) streamlines

(b) *The unsteady problem*

The problem is that of unsteady flow in a channel, with inlet and outlet conditions as shown in Figure 35. This problem has been solved by Hughes, Liu and Brooks[1] who: (i) unfortunately did not indicate the details of the mesh (number of elements, etc.) except to indicate that penalty-based 9 and 4 noded elements were used, (ii) presented results using Gauss–Legendre integration of the convection term, which they believed to demonstrate 'the inappropriateness' of such an integration of the convection term, and (iii) presented results using an 'upwinding' scheme which were stable and smooth for *both* Reynolds number values of $Re = 200$ and 10^7. In this regard, it is to be mentioned that Leone and Gresho[17] estimate the effective Re in this upwinded simulation to be 85 and $O(10^2)$. Results of a problem of

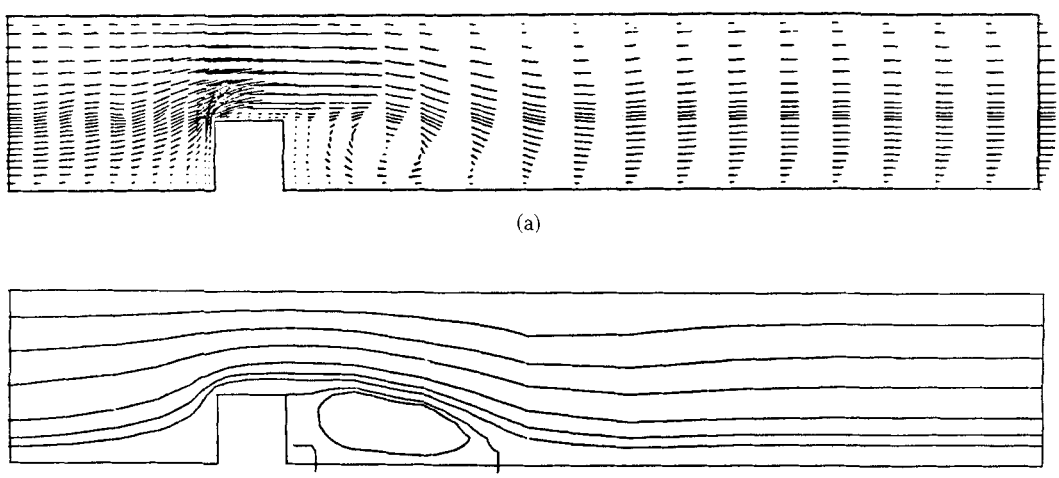

(a)

(b)

Figure 48. Unsteady flow at $Re = 200$, $t = 2{\cdot}0$ s: (a) velocity vectors; (b) streamlines

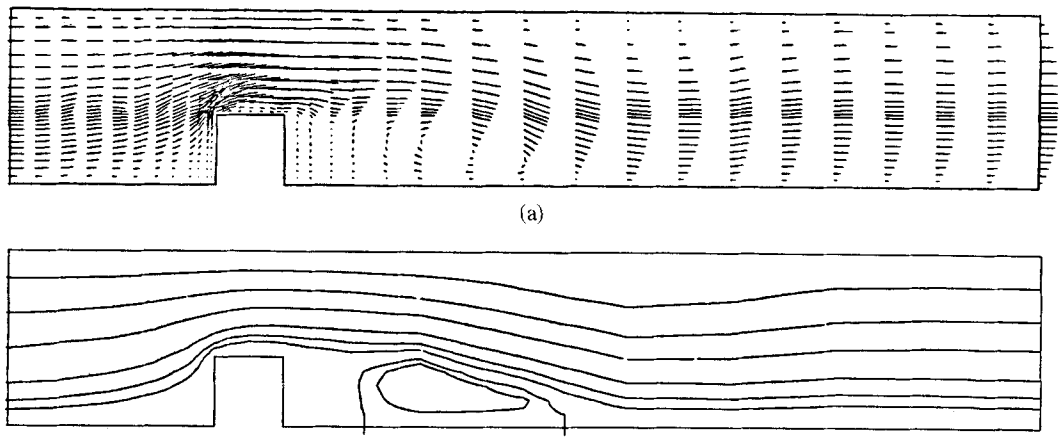

(a)

(b)

Figure 49. Unsteady flow at $Re = 200$, $t = 3{\cdot}0$ s: (a) velocity vectors; (b) streamlines

unsteady flow over a square step were also presented by Bercovier and Engelman[2] who, although not using any upwinding, present rather stable-appearing results, but unfortunately the *Re* number of the flow is not indicated.

The presently used finite element mesh for $Re = 85$ is shown in Figure 41, which has 199 four-noded elements and 237 nodes with a total of 673 equations prior to the imposition of boundary conditions. The inlet velocity v_x is uniform, as in Reference 1, and the channel length is 4 units.

The presently computed results for both velocity vectors and stream lines at $Re = 85$, and at times $t = 1{\cdot}0$, $2{\cdot}0$, $3{\cdot}0$, and $4{\cdot}0$ s, respectively, are shown in Figures 42–45. The eddy length at $t = 4{\cdot}0$ s, shown in Figure 45, is in excellent agreement with the directly obtained steady-state solution shown in Figure 39.

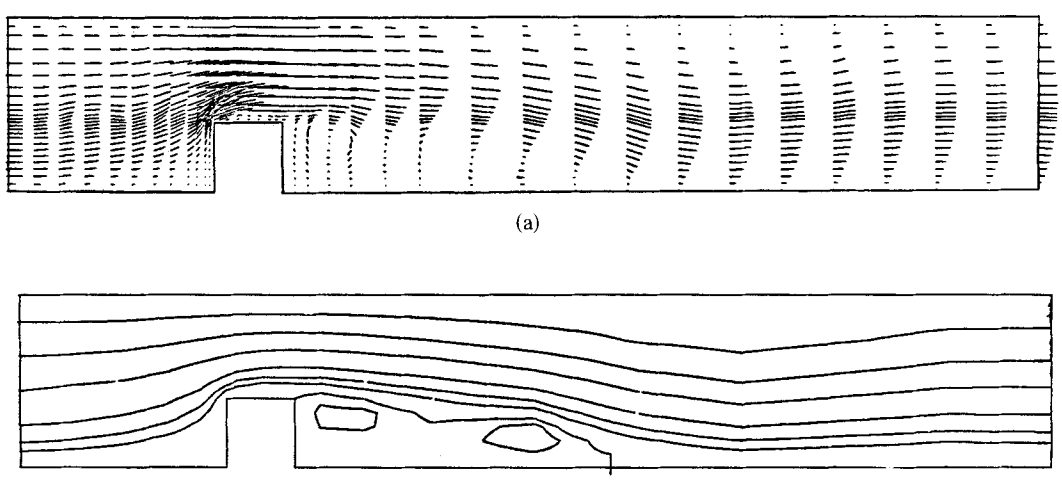

(a)

(b)

Figure 50. Unsteady flow at $Re = 200$, $t = 4{\cdot}0$ s: (a) velocity vectors; (b) streamlines

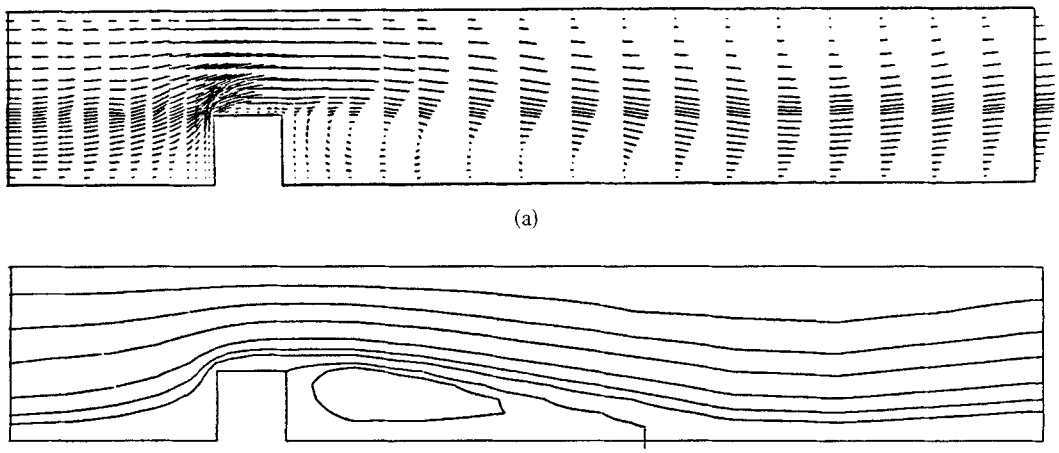

Figure 51. Unsteady flow at $Re = 200$, $t = 5{\cdot}0$ s: (a) velocity vectors; (b) streamlines

A second case of unsteady flow at $Re = 200$ was considered, with the finite element model being shown in Figure 46, with 659 equations, and a channel length of 6 units. The computed results for velocity vectors and streamlines, at $t = 1{\cdot}0$, $2{\cdot}0$, $3{\cdot}0$, $4{\cdot}0$, $5{\cdot}0$ and $6{\cdot}0$ s are shown in Figures 47–52, respectively. A curious, and as yet unexplained, feature of the present solution is the appearance of two eddies at $t = 4{\cdot}0$ s, which appear to coalesce at later times. The length and intensity of the eddy at $t = 6{\cdot}0$ s are in excellent correlation with those in the directly obtained steady-state solution shown in Figure 40.

Further testing of the present method is under way and the results will be reported elsewhere.

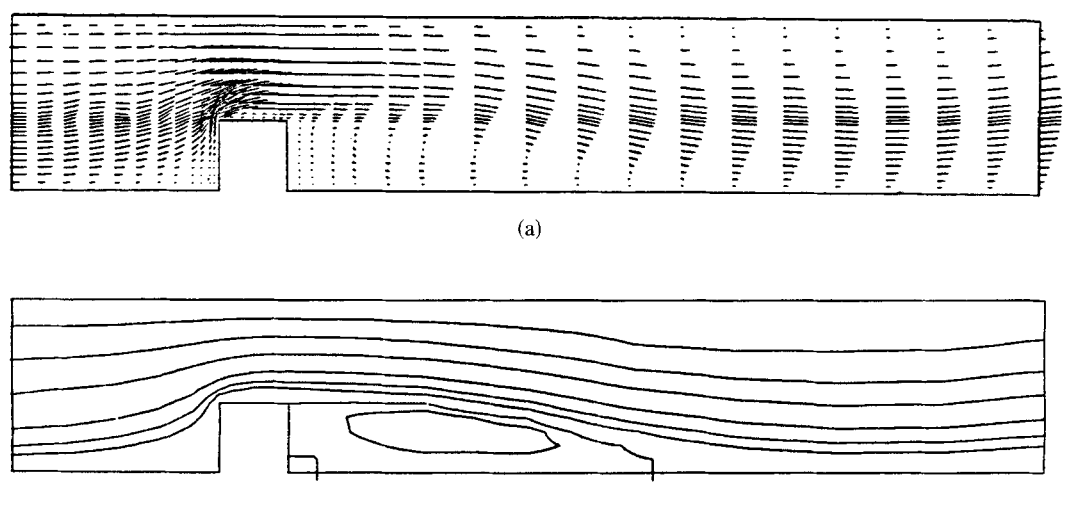

Figure 52. Unsteady flow at $Re = 200$, $t = 6{\cdot}0$ s: (a) velocity vectors; (b) streamlines

CONCLUSIONS

Even though we are unprepared to make any precise mathematical statements as to the rate of convergence of the present method, etc. we believe that the above numerical results indicate: (i) the relative efficiency of the present mixed method based on 'assumed deviatoric stress–velocity–pressure' over 'the selective-reduced-integration-penalty' methods or the mixed method based on 'assumed velocity–pressure'; (ii) the versatility of the present method in treating convective acceleration terms *without* resorting to 'upwinding'. Work that may enable us to give more mathematical estimates of convergence, is currently under way and will be reported elsewhere.

ACKNOWLEDGEMENTS

The above results were obtained during the course of investigations supported by AFOSR under grant 81-0057b to Georgia Tech. The authors gratefully acknowledge this support as well as the personal encouragement of Dr. A. Amos. The authors are also pleased to thankfully acknowledge the assistance of Ms. B. Bolinger in the preparation of this paper.

REFERENCES

1. T. J. R. Hughes, W. K. Liu and A. Brooks, 'Finite element analysis of incompressible viscous flows by the penalty function formulation', *J. Comp. Phys.* **30,** 1–60 (1979).
2. M. Bercovier and M. Engelman, 'A finite element simulation of viscous incompressible flows', *J. Comp. Phys.* **30,** 181–201 (1979).
3. J. C. Heinrich and R. S. Marshall, 'Viscous incompressible flow by a penalty function finite element method', *Computers and Fluids,* **9,** 73–83 (1981).
4. P. M. Gresho, C. D. Upson, S. T. Chan and R. L. Lee, 'Recent progress in the solution of time-dependent, three-dimensional, incompressible Navier–Stokes equations', T. Kawai (Ed.) *Finite Element Flow Analysis,* University of Tokyo Press, 1982, pp. 153–162.
5. J. N. Reddy, 'Analysis of three-dimensional incompressible flows by a penalty-finite-element method', in T. Kawai (Ed.) *Finite Element Flow Analysis,* University of Tokyo Press, 1982, pp. 37–44.
6. J. T. Oden, N. Kikuchi and J. Y. Song, 'Penalty-finite element methods for the analysis of Stokesian flows', *Computational Methods in Applied Mechanics and Engineering* (to appear).
7. J. T. Oden and O. Jacquotte, 'A stable second-order accurate, finite element scheme for the analysis of two-dimensional incompressible viscous flows', in T. Kawai (Ed.), *Finite Element Flow Analysis,* University of Tokyo Press, 1982, pp. 19–25.
8. O. R. Burgraff, 'Analytical and numerical studies of the structure of steady, separated flows', *Journal of Fluid Mechanics,* **24,** 113–151 (1964).
9. J. Donea, S. Giuliani, H. Laval and L. Quartapelle, 'Finite element solution of the unsteady Navier-Stokes equations by a fractional step method', *Comp. Meth. Appl. Mech. Eng.* **30,** 53–73 (1982).
10. T. J. R. Hughes, R. L. Taylor and J.-F. Levy, 'High Reynolds number, steady, incompressible flows by a finite element method', in J. T. Oden, C. Taylor and O. C. Zienkiewicz (Eds) *Finite Elements in Fluids,* **3,** Wiley, 1978, pp. 55–73.
11. M. S. Engelman, G. Strang and K. J. Bathe, 'The application of quasi-Newton methods in fluid mechanics', *Int. J. Num. Meth. Eng.* **17,** 707–718 (1981).
12. D. K. Gartling, R. E. Nickell and R. I. Tanner, 'A finite element convergence study for accelerating flow problems', *Int. J. Num. Meth. Eng.* **11,** 1155–1174 (1977).
13. G. K. Batchelor, *An Introduction to Fluid Mechanics,* Cambridge University Press, Cambridge, 1970.
14. M. K. Denham and M. A. Patrick, 'Laminar flow over a downstream-facing step in a two-dimensional flow channel', *Trans. Inst. Chem. Engineers,* (Britain) **52,** 361–367 (1974).
15. D. J. Atkins, S. J. Maskell and M. A. Patrick, 'Numerical prediction of separated flows', *Int. J. Num. Meth. Eng.* **15,** 129–144 (1980).
16. C. E. Thomas, K. Morgan and C. Taylor, 'A finite element analysis of flow over a backward facing step', *Computers and Fluids,* **9,** 265–278 (1981).
17. J. M. Leone, Jr. and P. M. Gresho, 'Finite element simulations of steady, two-dimensional, viscous incompressible flow over a step', *J. Comp. Phys.* **32,** 167–191 (1981).